Computational Particle Mechanics (2022) 9:537–550
https://doi.org/10.1007/s40571-021-00427-9

Impact dynamics and power-law scaling behavior of wet agglomerates

Thanh-Trung Vo[1] · Cuong T. Nguyen[2,3] · Trung-Kien Nguyen[4] · Van My Nguyen[5] · Thi Lo Vu[6,7]

Received: 22 March 2021 / Revised: 27 May 2021 / Accepted: 11 June 2021 / Published online: 30 June 2021

Abstract
We investigate the impact dynamics of a single wet agglomerate composed of primary spherical particles impacting a flat plane by using three-dimensional discrete element method simulations. The primary particle is assumed to be rigid and interacted with its near-neighboring particles by introducing approximate analytical expressions of capillary cohesion forces and lubrication forces induced from the liquid in addition to their elastic and frictional interactions. The paper analyzes the mechanical strength, the deformation, and the connectivity of wet particle agglomerate during the impact as well as in its early-stage impact and the final-stage deposition. We show that the mechanical strength, deformation, and connectivity of granule strongly depend on the key parameters (the liquid–vapor surface tension, the liquid viscosity, and the impact speed of agglomerate). In particular, the early-stage strength and the height of wet agglomerate at its final-stage deposition nicely behave as a function of the Capillary–Stokes inertial number that combines the Capillary number and Stokes number, and the macroscopic strength of the agglomerate at its early-stage impact has the microscopic origin from the normal compressive forces between primary particles. These observations are consistent that represent the relationship between the rheological properties and the liquid properties and the impact conditions of wet granular materials.

Keywords Granular matter · Agglomerate · Discrete element method · Impact · Capillary number · Stokes number

1 Introduction

Wet agglomerates are a common type of granular materials either naturally formed by the action of capillary bridges between primary particles [1,2], or as industrial products in the agglomeration processes in steel-making [3–6], pharmaceutical, and food industries [7,8]. The physical and mechanical properties of such agglomerates depend on the discrete nature of material including primary particles and the binding liquid [9–17] as well as its collisional type [17–19]. Under the action of external forces due to contacting with surrounding particles [3,16,20–23], impacting with the drum walls [24], or colliding with the containing walls during storage [25], the mechanical strength of agglomerates changes and these agglomerates could also be deformed or disintegrated or rebounded depending on both of impact conditions and the interactions between primary particles inside agglomerates [18,26–32]. These interactions become more complex when both cohesive and viscous effects of the binding liquid come into play in addition to the elastic and frictional contacts [17,33]. Therefore, the prediction of the physical and mechanical behavior of cohesive granular materials such as wet particle agglomerates based on such

✉ Thanh-Trung Vo
trungvt@dau.edu.vn

✉ Thi Lo Vu
vuthilo@tdtu.edu.vn

1 Bridge and Road Department, Danang Architecture University, Da Nang City, Vietnam

2 Faculty of Vehicle and Energy Engineering, Phenikaa University, Hanoi 12116, Vietnam

3 Phenikaa Research and Technology Institute (PRATI), No. 167 Hoang Ngan, Trung Hoa, Cau Giay, Hanoi 11313, Vietnam

4 Faculty of Building and Industrial Construction, National University of Civil Engineering, Hanoi, Vietnam

5 Faculty of Road and Bridge Engineering, University of Science and Technology – The University of Danang, 54 Nguyen Luong Bang Street, Lien Chieu District, Da Nang City, Vietnam

6 Division of Computational Mathematics and Engineering, Institute for Computational Science, Ton Duc Thang University, Ho Chi Minh City, Vietnam

7 Faculty of Civil Engineering, Ton Duc Thang University, Ho Chi Minh City, Vietnam

complex interactions and impact loads plays an important role.

We study the case in which a single wet agglomerate impacts on a flat plane from its original height by considering a homogeneous distribution of the binding liquid inside the granule. Upon impact, the particles start moving as a result of occurring the relative displacements between particles and the external pressure such as particle gravity [34]. These collective movements generate the inertial stress $\sigma_{\mathrm{i}} \sim \rho\langle d\rangle^2\dot{\gamma}^2$, where ρ is the particle density, $\langle d\rangle$ is the mean particle diameter, and $\dot{\gamma}$ denotes the impact rate (or shear rate in granular flow) [35,36]. Due to the presence of the capillary bonds between particles in contact and the domination of the cohesive stress $\sigma_{\mathrm{c}} \sim \gamma_s/\langle d\rangle$ and viscous stress $\sigma_{\mathrm{v}} \sim \eta\dot{\gamma}$ as compared to the particle gravity, the physical and mechanical properties of wet agglomerates are expected dependently on the actions of σ_{i}, σ_{c}, and σ_{v} or their dimensionless parameters: the Capillary number Ca and the Stokes number St, where γ_{s} is the liquid–vapor surface tension, η is the liquid viscosity. The Capillary number Ca is the ratio of the viscous stress σ_v to the cohesive stress σ_{c} ($\mathrm{Ca} = \sigma_{\mathrm{v}}/\sigma_{\mathrm{c}}$). The Stokes number St is the ratio of the σ_{i} and σ_{v} ($\mathrm{St} = \sigma_{\mathrm{i}}/\sigma_{\mathrm{v}}$).

Studying the physical and mechanical responses of a single agglomerate impacting a plane is represented via the evolution of the granule strength, breakage, deformation at its early-stage impact and final-stage deposition as well as during the impact. The wet agglomerate could still survive or disintegrate (or fully spread) at its final deposition stage depending on the nature properties of the binding liquid characterized by the cohesive and viscous stresses, the raw materials, and the impact condition [16,37]. The mechanical strength of agglomerate increases proportionally to the cohesive stress and the connectivity of agglomerates that expressed as an analytical model [14]. Such agglomerate also deforms as a consequence of irreversibly breaking of capillary bridges between near-neighboring particles [14,17,38,39]. All of these behaviors are expected to be controlled by the combinations of the cohesion and viscosity of the liquid bridges and the impact speed of wet agglomerate.

In fact, the combination of the cohesive and viscous effects of the binding liquid and the flow rate of wet granular materials have been introduced for different configurations in recent years. In pressure-controlled condition and free surface flows of cohesive granular materials, the cohesive stress strongly affects the rheology of such flows, and a combination of the inertial number I (defined as a square root of the ratio of σ_{i} and the confining stress σ_{n}) and the cohesion index ξ, defined as a ratio of σ_{c} and σ_{n}, can be used to scale the rheology of cohesive granular flows and the evolution of wet agglomerate characterized by its elongation, erosion, and breakage [17]. Similarly, when the lubrication effects come into play with the inertial effects of granular materials, a combination of I and the Stokes number St can be used to scale the effective viscosities of the dense suspension [40] or the visco-inertial granular flows [41,42]. Remarkably, Vo and coworkers [33] found the additive mechanism of cohesive force and viscous force in addition to the inertial force in each particle interaction. The rheological properties of complex granular flows characterized by the effective friction coefficient and packing fraction as well as the texture variables nicely collapse as a function of a modified inertial number which combines I, ξ, and St. However, the model of wet particle agglomerates impacting a flat plane in this current work is a very different case as compared to the configuration of unsaturated granular flows, and whether the physical and mechanical responses of impact agglomerate can be described by a dimensionless parameter as above examples?

In this paper, the behavior of a single wet agglomerate impacting a rigid plane is studied by means of 3D discrete element method (DEM) simulations. The simulations were performed by using an approximate analytical expression of the capillary attraction forces and lubrication forces between near-neighboring particles having the gap no exceed a rupture distance in addition to the elastic and frictional forces at their contacts. We investigate the evolution of the mechanical strength at the early-stage plastic threshold and the deformation and connectivity at the final-stage deposition of the wet agglomerate by systematically varying a broad range of values of the liquid–vapor surface tension, the liquid viscosity, and the impact velocity. As we shall see, a nontrivial combination of the control parameters as a new dimensionless inertial number can scale the mechanical and physical properties of impact agglomerate.

In the following, we first give the physical assumptions and the numerical approach and generate the impact test in Sect. 2. Then, in Sect. 3, we analyze the mechanical strength, the deformation, the connectivity, and the final-stage deposition height of granule as a function of the impact speed. In Sect. 4, we introduce the power-law scaling behavior of impact agglomerate. Finally, we conclude in Sect. 5 with an impressive summary of noteworthy results and its possible extensions.

2 Numerical method and model preparation

Our numerical simulations are performed by means of the discrete element method (DEM) with an approximate analytical expression of the cohesive forces and the viscous forces as a function of separation distance between particles in addition to the elastic and frictional forces at their contacts. We first describe below the physical assumptions of the distribution and transport of the binding liquid underlying the impact model. Then, we introduce briefly the numerical algorithm and the model of the impact test of an agglomerate.

2.1 Physical assumptions

The DEM has been extensively used for the simulations of granular materials due to the advantage of providing access the particle interactions and easily varying broad range of values of the system parameters. The equations of motion of all particles are integrated according to the explicit stepwise scheme by taking into account the particle interactions [43–45]. In advanced DEM, it is possible to implement the liquid–solid interactions in addition to the solid–solid contacts [34,46]. This approach requires the substantial particle computation of the liquid phase as well as the model for the transition of gas–liquid phase [41,47,48]. However, such model also requires much more computational cost and memory in order to discretize the liquid phase. For this reason, a balance between computational efficiency and physical realism is considered in advanced DEM simulations. In the "pendular" state of the binding liquid, it is found to represent the liquid phase by an approximate analytical expression of the capillary attraction forces and lubrication forces between particles having no exceed a debonding distance as well as considering a particle-scale model for the distribution and transport of the liquid [16,17,49].

The presence of the binding liquid inside agglomerates as the liquid clusters is naturally formed due to the condensation from a liquid vapor or mixing the liquid with the particles. For low amounts of the liquid in the pendular regime, the liquid is in the form of the binary bridges. As the liquid volume increases, the liquid cluster has more and more particles. In the thermodynamic equilibrium of the liquid, the liquid is homogeneously distributed and the cohesion forces of the binding liquid are controlled by the wetted surface of particles and the Laplace–Young pressure. In non-equilibrium state, the liquid is not uniformly distributed in granular packing. However, in our simulations, we do not consider the wetting and dispersion processes of the binding liquid, which represented in the nucleation step of agglomerates. This means the liquid is assumed to be initially homogeneous distributed inside wet agglomerates.

In practice, a part of an amount of the liquid is absorbed into the rough surface of primary particles, and this liquid volume is not involved in capillary bridges between particles. As a wet agglomerate falls down and impacts on a rigid plane at a high speed, the capillary bond between particles may be broken when the separation distance between particles exceeds their rupture distance, the liquid is then immediately shared proportional to the particle size due to the lubrication effects of the liquid, and this liquid volume is assumed to be mainly covered the particle asperities without re-forming [46,50]. This simplification allows us to investigate the effects of liquid properties and impact velocity on the physical and mechanical responses of wet particle agglomerates. It is also worth introducing here that these above assumptions have been used for the simulations of the coalescence of granules during collision [9], the agglomeration of wet particles [16], the impact breakage of agglomerates [10,11,13,51], and diametrical compression test of spherical agglomerates [12,14]; these results were almost in agreement with experimental works.

2.2 Discrete element method

The discrete element method (DEM) has been used for simulations of the granular materials in many applications in different scientific fields including soil mechanics, soft matter physics, powder technology, and geological processes over the last forty years [43,52–55]. In the DEM, each particle is modeled as a rigid grain and interacts with its near-neighboring particles via the normal and tangential forces [43,55]. In order to calculate the interactions between particles, a time discretized form and a large repulsive stiffness of particles of this discrete approach are required [43]. The contact forces between particles are proportional to their normal and tangential relative displacements, and these particle movements are obtained by considering the step-wise integration based on the Newton second law. The equations of translational and rotational motion of a particle i with its radius R_i are obtained by integrating all forces including contact forces and liquid forces exert on particle i [43,54].

$$
\begin{aligned}
m_{\mathrm{i}} \frac{\mathrm{d}^2 \mathbf{r}_{\mathrm{i}}}{\mathrm{d}t^2} &= \sum_{\mathrm{j}} [(f_{\mathrm{n}}^{ij} + f_{\mathrm{c}}^{ij} + f_{\mathrm{v}}^{ij})\mathbf{n}^{ij} + f_{\mathrm{t}}^{ij}\mathbf{t}^{ij}] + m_{\mathrm{i}}\mathbf{g}, \\
\mathbf{I}_{\mathrm{i}} \frac{\mathrm{d}\boldsymbol{\omega}_{\mathrm{i}}}{\mathrm{d}t} &= \sum_{\mathrm{j}} f_{\mathrm{t}}^{ij} \mathbf{c}^{ij} \times \mathbf{t}^{ij},
\end{aligned} \tag{1}
$$

where i and j are two particles in contact and m_{i} and $\boldsymbol{r}_{\mathrm{i}}$ are the mass and position of particle i, respectively. $\mathbf{I}_{\mathrm{i}}$ and $\boldsymbol{\omega}_{\mathrm{i}}$ denote the inertia matrix and angular velocity vector, respectively, and $\boldsymbol{g}$ denotes the gravitational acceleration vector. $\mathbf{n}^{ij}$ and $\mathbf{t}^{ij}$ are the normal and tangential unit vectors, respectively. Meanwhile, $\mathbf{n}^{ij}$ has the direction pointing from particle j to particle i, and the tangential unit vector has the direction opposite to the relative tangential displacement between these two particles. $\mathbf{c}^{ij}$ is another unit vector pointing from the center of particle i to the contact point with particle j. In this current work, the equations of motion of all particles are assimilated by using a velocity Verlet time-stepping scheme [17,43,56].

In Eq. (1), the normal contact force f_n is calculated as a linear combination of the normal elastic force and normal damping force between two particles i and j [43,57], and this means that the effects induced by the deformation at the contact are negligible as compared to the effects of cohesion

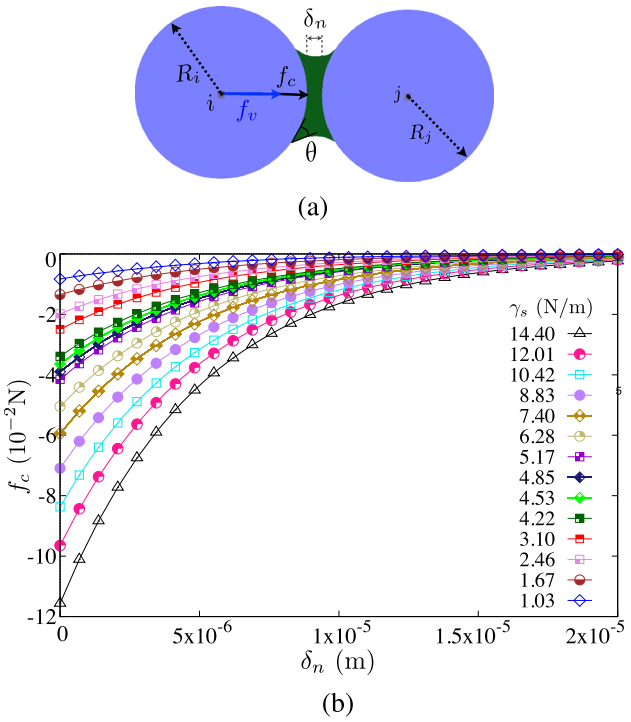

Fig. 1 **a** A schematic drawing representation the capillary bond with the different forces acting between particle i and its neighboring particle j, **b** capillary attraction force f_c plotted as a function of the normal elastic deflection distance δ_n up to the cutoff distance d_c between particles i and j for different values of the liquid–vapor surface tension γ_s

and the contact viscosity.

$$f_n = f_n^e + f_n^d \,. \tag{2}$$

where $f_n^e = k_n \delta_n$ is the normal elastic force, expressed as a linear function of the normal elastic deflection δ_n at the contact point, k_n denotes the normal stiffness, and $f_n^d = \gamma_n \dot{\delta}_n$ denotes the damping force that is proportional to the relative normal velocity $\dot{\delta}_n$, where γ_n is the normal viscous damping. These contact forces occur only when $\delta_n < 0$, and this means that there is an overlap between particles in contact.

The tangential force f_t is obtained by considering the Coulomb friction law, and this force is the sum of a tangential elastic force $f_t^e = k_t \delta_t$ and a tangential damping force $f_t^d = \gamma_t \dot{\delta}_t$, where k_t and γ_t denote the tangential stiffness and the tangential viscous damping parameter, respectively, and $\dot{\delta}_t$ denotes the tangential velocity, obtained as a derivation of the relative tangential displacement δ_t. According to the Coulomb friction law, the tangential force is the minimum value between (μf_n) and the sum of the tangential elastic force $k_t \delta_t$ and tangential damping one $\gamma_t \dot{\delta}_t$ [39,43,54]:

$$f_t = -\min\left\{(k_t \delta_t + \gamma_t \dot{\delta}_t), \mu f_n\right\}. \tag{3}$$

As mentioned above, the liquid is in the form of the capillary bonds between spherical particles [14,58]. This binding liquid is assumed to be homogeneously distributed in the initial state of wet particle agglomerate. In our simulations, the capillary bridges are characterized by the liquid–vapor surface tension and the liquid viscosity. These nature properties of the liquid induce the capillary attraction forces and viscous forces [16,33,59]. These cohesive and viscous forces tend to increase the mechanical strength of the agglomerate. In this current work, we assumed that the binding liquid can be broken irreversibly due to the drainage and absorption on the particle rough surface. This means that the capillary bridges cannot be reformed during the test.

The capillary attraction force f_c between two near-neighboring particles is proportional to the volume V_b of the capillary bond, the liquid–vapor surface tension γ_s, and the solid–liquid–gas contact angle θ. In our simulations, θ is set to zero as a consequence of considering the full covering of the liquid binding on the particle surface. The capillary cohesion force f_c is an approximate solution of the Laplace–Young equation [60–62], as given following and plotted in Fig. 1:

$$f_c = \begin{cases} -\kappa\ R, & \text{for } \delta_n < 0, \\ -\kappa\ R\ e^{-\delta_n/\lambda}, & \text{for } 0 \le \delta_n \le d_c, \\ 0, & \text{for } \delta_n > d_c, \end{cases} \tag{4}$$

where $R = \sqrt{R_i R_j}$ is the geometrical mean radius of two particles radii R_i and R_j and κ is the capillary force prefactor, as given by:

$$\kappa = 2\pi \gamma_s \cos\theta. \tag{5}$$

This cohesion force was found to provide an excellent agreement with experimental data on the cohesion of wet granular materials [62]. The cutoff distance d_c is given by [46]

$$d_c = \left(1 + \frac{\theta}{2}\right) V_b^{1/3} \,. \tag{6}$$

λ (in Eq. 4) is the characteristic length, illustrated the exponential fall-off of the capillary attraction force, as given following:

$$\lambda = c\ h(r)\ \left(\frac{V_b}{R'}\right)^{1/2}, \tag{7}$$

where $R' = 2R_i R_j/(R_i + R_j)$ denotes the harmonic mean radius between particles i and j, $r = \max\{R_i/R_j;\ R_j/R_i\}$ is the size ratio between two primary particles i and j, $h(r) = r^{-1/2}$, and $c \simeq 0.9$ [57,62]. Figure 1b displays the capillary cohesion force f_c, plotted as a function of the normal elastic deflection distance δ_n up to the cutoff distance d_c between two

near-neighboring particles for different values of the surface tension of the binding liquid.

The normal liquid viscous force f_v in each capillary bond between two primary particles is proportional to the viscosity of the liquid η, the particle size, and the relative normal velocity v_n, obtained by taking a derivation of the normal elastic deflection distance δ_n, but it is inversely proportional to the gap between two particles [16,17,33,42], as given by:

$$f_v = \frac{3}{2}\pi R^2 \eta \frac{v_n}{\delta_n}, \tag{8}$$

where v_n is a negative value when the normal elastic deflection distance is increasing. In the viscous points of view, the liquid viscous force tends to diverge when δ_n tends to zero. In order to prevent this divergence behavior of the lubrication forces, the characteristic length δ_0 is defined, reflecting the roughness of the particle surface. For the positive separation distance ($\delta_n > 0$),

$$f_v = \frac{3}{2}\pi R^2 \eta \frac{v_n}{\delta_n + \delta_0}. \tag{9}$$

The liquid viscous force is obtained as a largest value when occurring the overlap between near-neighboring particles ($\delta_n \leq 0$),

$$f_v = \frac{3}{2}\pi R^2 \eta \frac{v_n}{\delta_0}. \tag{10}$$

Similar to the cohesive force, the viscous force f_v is expressed as a function of the normal elastic deflection distance δ_n up to the cutoff distance d_c between two particles for a given value of v_n for different values of η, as shown in Fig. 2. As already mentioned above, the relative normal velocity v_n can be positive or negative corresponding to the contraction and extension of the binding liquid.

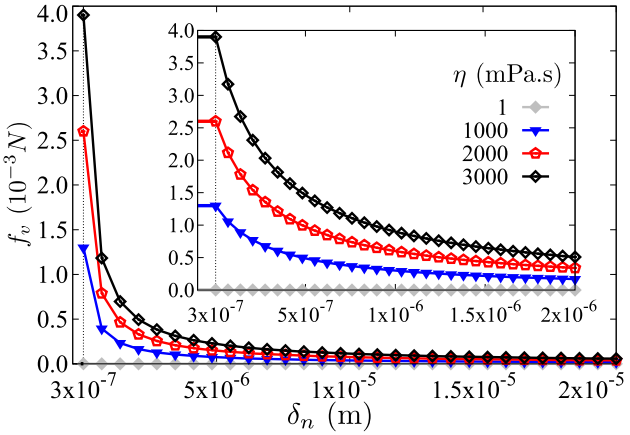

Fig. 2 Lubrication force f_v plotted as a function of the normal elastic deflection distance δ_n up to the cutoff distance d_c between two primary particles for different values of the viscosity η of the binding liquid and a given value of the relative normal velocity v_n (5×10^{-3} m/s)

2.3 Impact test

In order to construct a spherical agglomerate of wet primary particles, we first prepared a large sample of nearly 70.000 spherical particles by means of isotropic compaction in a cube. We introduced a weak size polydispersity by uniformly varying the particle diameter in a range $d_{max} = 2d_{min}$. The particle size distribution is assumed to be uniformed by particle volume fraction. The particle diameter is divided into three different size classes, and all the size classes have the same volume, i.e., a small number of large particle sizes and a large number of small particle sizes. This distribution leads to a dense granular packing due to the filling of small particles to the pore spaces between large particles. After all spherical particles reached an equilibrium state in the case of without considering the capillary attraction forces and viscous forces, a spherical probe was introduced in the center of the cube and its diameter was increased until reaching exactly 31.470 spherical particles inside the probe. Then, these spherical particles were extracted and the cohesive forces and viscous forces were activated between neighboring particles until reaching once more equilibrium state.

To investigate the mechanical strength, deformation, and connectivity of wet particle agglomerates at its early-stage, final deposition stage, and during the transition, we performed impact test, by leaving a wet agglomerate from a height that equals a half of its radius, measured from the lowest point of the agglomerate to a flat plane, as shown in Fig. 3. We ran totally 234 simulations by systematically varying the liquid–vapor surface tension γ_s in a broad range [1.0, 14.4] N/m, the liquid viscosity η in a range [1.0, 3000.0] mPa s, and the initial velocity v_0 in a range [1.0, 5.0] m/s with the gravity set to $g = 9.81$ m/s^2. The impact velocity v_i is at the impact time when the agglomerate starts colliding with the plane. The friction coefficient between primary particles and between particle and plane was set to 0.5. All the system parameters are given in Table 1. The data points presented in the following are average values for the agglomerate strength or extracted as a single value for the deposition and connectivity of such agglomerate.

Figure 4 displays the evolution of mean particle velocity v as a function of $t \times g/v_0$ for different values of the liquid–vapor surface tension γ_s of capillary bridges with a given value of the liquid viscosity η and the initial impact velocity v_0. All primary wet particles are first assigned an initial velocity v_0 at their original positions. The granule falls down with a velocity that slightly increased due to the effects of particle gravity and then interacts with the plane at an impact velocity v_i. The agglomerate velocity then declines rapidly and undergoes the deposition stages due to the effects of liq-

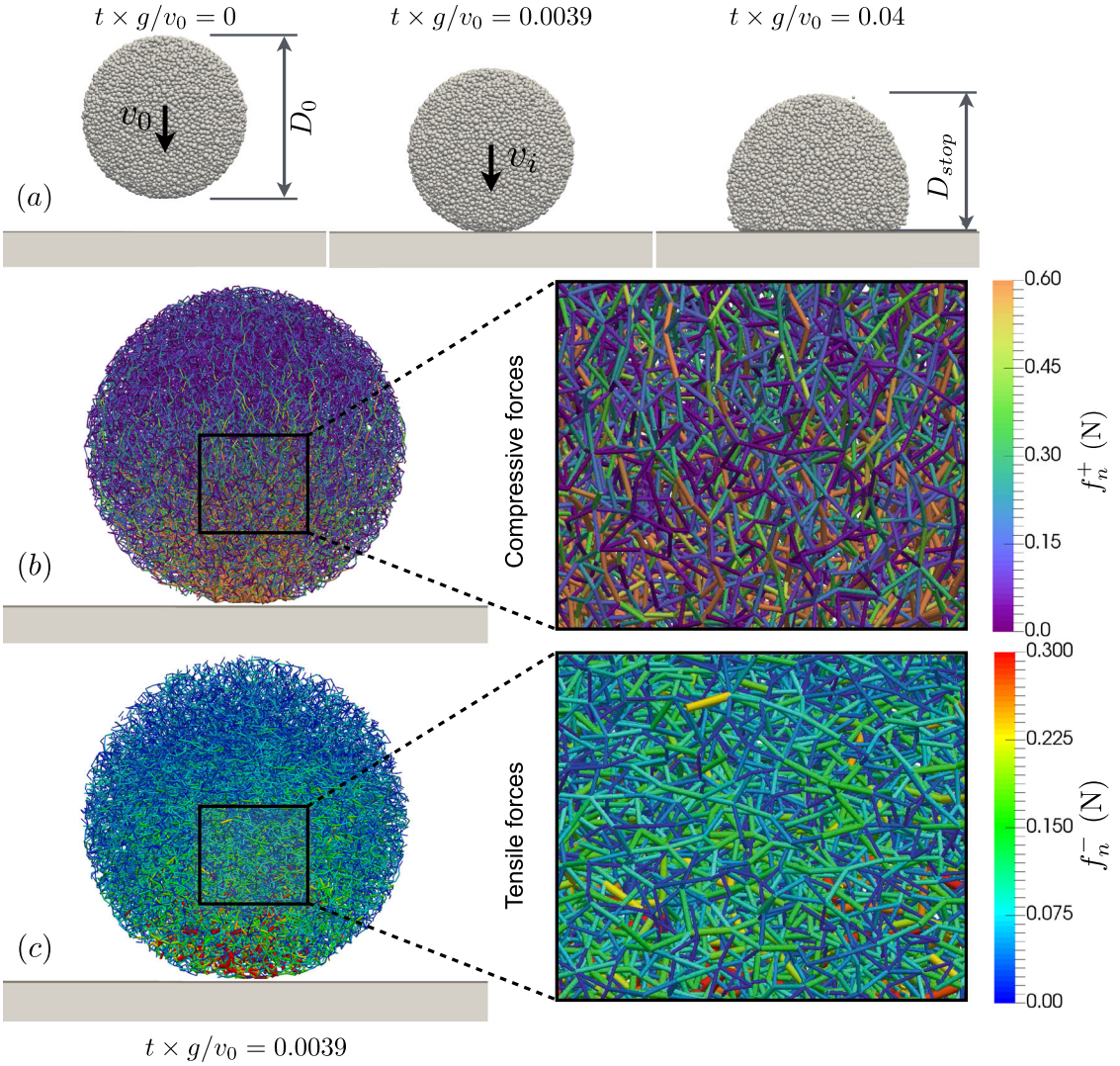

Fig. 3 **a** Snapshots of a wet agglomerate impacting a rigid plane and evolution of granule deformation from initiation to the final-stage deposition for a given value of the liquid–vapor surface tension ($\gamma_s = 14.4$ N/m), the liquid viscosity ($\eta = 3000$ mPa s), and the initial velocity $v_0 = 4.0$ m/s. **b** Compressive and **c** tensile force chains of agglomerate at the early-stage impact, respectively

Table 1 Systematic parameters used in the simulations

Parameter	Symbol	Value	Unit
Largest particle diameter	$d_{\max}$	1200	μm
Particle density	ρ	2600	kg/m^3
Coefficient of friction	μ	0.5	
Normal stiffness	k_n	10^6	N/m
Tangential stiffness	k_t	8×10^5	N/m
Normal damping	γ_n	0.5	Ns/m
Tangential damping	γ_t	0.5	Ns/m
Time step	Δt	2×10^{-8}	s

uid properties and the dissipation of particle energy via the solid and liquid interactions. This declination rate is proportional to the surface tension γ_s of the liquid. The granule then reaches the stable state (the final-stage deposition) at the end of the impact test more or less fast depending on the cohesion of the liquid.

During an impact, the mechanical strength of wet particle agglomerate changes as a consequence of occurring the relative displacements and interactions between particles. The vertical stress σ_{zz} of wet particle agglomerate can be obtained by considering the normal forces and the branch vectors joining the particle centers:

$$\sigma_{zz} = \frac{1}{V_a} \sum_{k=1}^{N_b} f_z^k \ell_z^k = n_b \langle f_z^k \ell_z^k \rangle_k, \tag{11}$$

where V_a is the volume of agglomerate, N_b denotes the number of capillary bonds in current step, f_z^k and l_z^k are the z-components of the force vector and branch vector of capillary bond k, respectively, and $n_b = N_b/V_a$ is the number density of the capillary bonds. The symbol $\langle \cdots \rangle_k$ denotes averaging over all contacts k in the volume.

Figure 5 shows the average vertical stress σ_{zz} that is expressed as a function of $t \times g/v_0$ for different values of γ_s and for a given value of the liquid viscosity and the impact velocity. The granule strength equals zero before occurring the impact with the plane corresponding to its initial stability. Then, the vertical stress soars immediately and reaches the early-stage plastic threshold. The time appearing the early-stage threshold is independent to the surface tension γ_s of the liquid, whereas the value of the stress threshold is proportional to γ_s. This can be explained due to the immediate increase in the contact forces between primary particles after receiving the collisional force at the contact point between agglomerate and the flat plane, whereas there is no enough time for the particle movements. The threshold is a signature of the plastic behavior of wet particle agglomerate due to the rearrangement of primary particles and the tensile effects of the capillary bonds, which have the direction perpendicular to the impact direction, as easily visualized in the zoom in Fig. 3c. After that, the granule stress declines rapidly as a consequence of irreversibly broken of the capillary bonds. As we can see, the speed of this declination and the stabilized achievement is proportional to γ_s, which represented via the speed of reaching the final-stage deposition, as shown in Fig. 5.

The average vertical stress of a wet particle agglomerate impacting a flat plane reflects the microstructure and the deformation of the granule, which depend on the liquid–vapor surface tension γ_s, the liquid viscosity η, and the impact velocity v_i. In our simulations, the granule deformation is characterized by the height D during the impact test, and the microstructure of wet agglomerate can be characterized by the number of loss capillary bridges Z_{lost}, defined as an average number of loss capillary bonds. Figure 6 displays D/D_0 as a function of $t \times g/v_0$ for broad range of values of γ_s and for a given value of $\eta = 3000$ mPa s and $v_0 = 4.0$ m/s, where D_0 is the initial diameter of agglomerate. For each

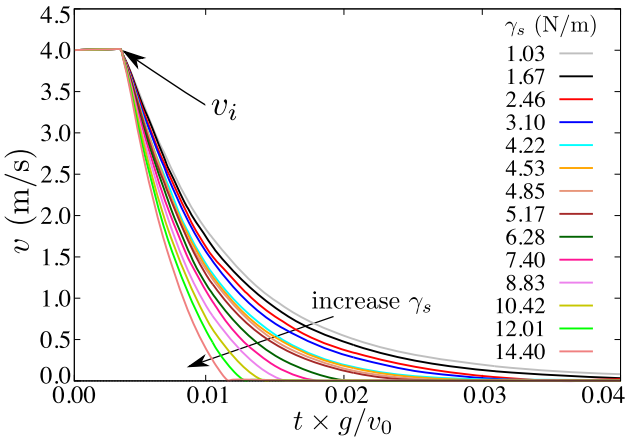

Fig. 4 Evolution of average velocity of primary particles for different values of the liquid–vapor surface tension γ_s for a given value of the liquid viscosity $\eta = 3000$ mPa s and the initial velocity $v_0 = 4.0$ m/s

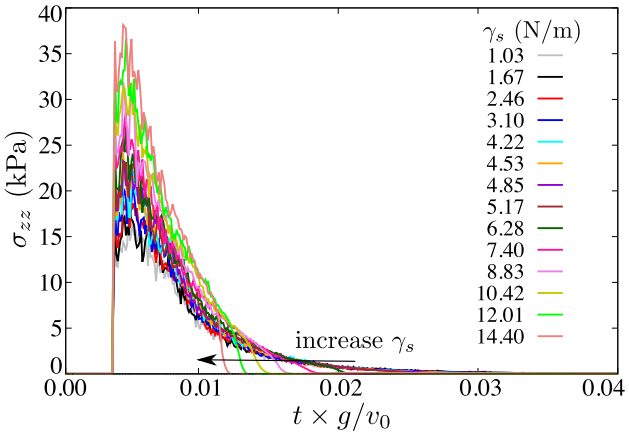

Fig. 5 Evolution of average vertical stress σ_{zz} as a function of time for different values of the liquid–vapor surface tension γ_s for a given value of the liquid viscosity $\eta = 3000$ mPa s and the initial velocity $v_0 = 4.0$ m/s

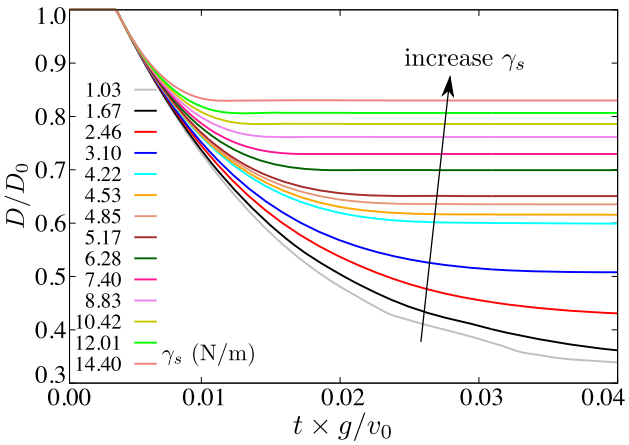

Fig. 6 The vertical size D of agglomerate normalized by its initial diameter D_0 as a function of $t \times g/v_0$ for different values of γ_s for a given value of the liquid viscosity $\eta = 3000$ mPa s and the initial velocity $v_0 = 4.0$ m/s

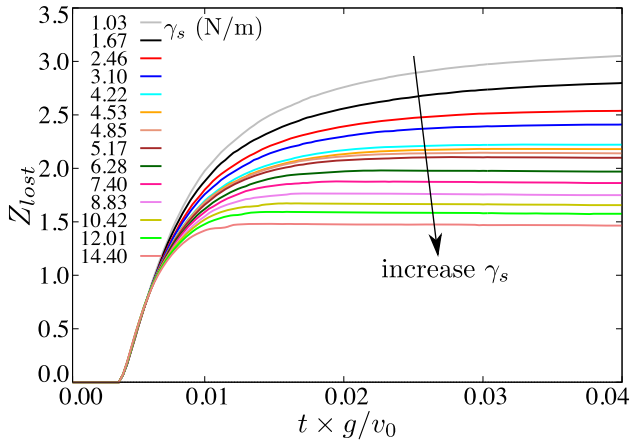

Fig. 7 Loss coordination number Z_{lost} of wet particle agglomerates as a function of $t \times g/v_0$ for different values of the liquid–vapor surface tension γ_s for a given value of the liquid viscosity $\eta = 3000$ mPa s and the initial velocity $v_0 = 4.0$ m/s

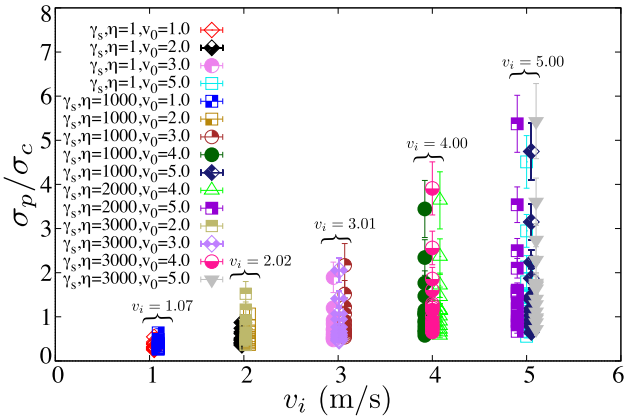

Fig. 8 Peak strength σ_{p} of agglomerates normalized by the cohesive stress $\sigma_{\text{c}} = \gamma_{\text{s}}/\langle d \rangle$ as a function of the impact velocity v_{i} for all of simulations. The error bars represent the standard deviation in each simulation during reaching plastic threshold. For each set of simulations, the symbols and their colors correspond to each value of η and v_{i} and varying γ_{s} in a broad range of values. (Color figure online)

value of the liquid–vapor surface tension γ_s, the granule has a final deposition height (or final deposition diameter) D_{stop}, and this increases proportionally to the surface tension of the liquid.

Figure 7 represents the evolution of the average number of loss capillary bonds Z_{lost} as a function of the time for different values of γ_{s}. Z_{lost} first increases rapidly when occurring the impact between agglomerate and plane. Then, this average number reaches a plateau in the deposition stages more less fast depending on the values of the liquid properties and the impact rate, and there is no more capillary bond broken in its final deposit stage. In the final-stage deposition, Z_{lost} decreases proportionally to γ_{s} of the binding liquid. This means that the granule is not abrupt rupture during the test, and it could be deformed or fully spread depending on the values of system parameters. Thus, the final deposition stage of the impact test is an important feature, which will be analyzed in more detail below.

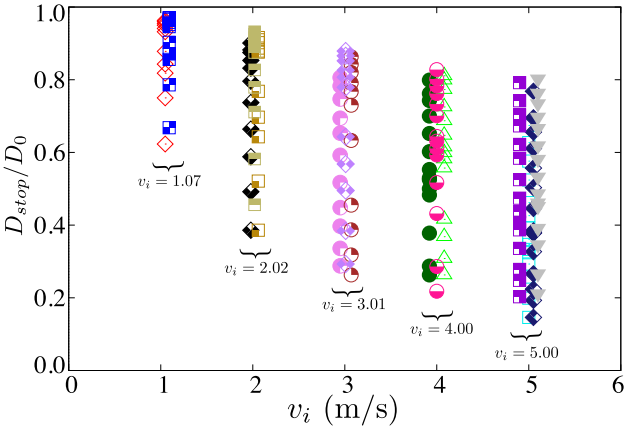

Fig. 9 Deposit vertical diameter D_{stop} normalized by initial diameter D_0 of wet agglomerates as a function of the impact velocity v_{i} for all of simulations. For each set of simulations, the symbols and their colors represent for each value of η and v_{i} and a broad range of values of γ_{s}. (Color figure online)

3 Mechanical strength and deposition of agglomerate

We now consider two more parameters (the liquid viscosity and the impact velocity) which are varied in different ranges of their values. Due to the observation of the ductile behavior of wet particle agglomerates, the plastic threshold σ_{p} is observed in all our numerical results by considering the average value of five data points closet to the peak value. Figure 8 displays the mean peak stress σ_{p} normalized by the cohesive stress $\sigma_{\text{c}} = \gamma_{\text{s}}/\langle d \rangle$ as a function of the impact velocity v_{i} for all our 234 simulations. The impact velocity v_{i} is obtained at the impact time when the lowest primary particles of the granules start touching the plane. In order to improve the visibility of the data points, we plotted them separately although they obtained at the same impact velocity v_{i}, as shown in Figs. 8, 9, and 10. As we can see, the granule strength increases proportionally to v_{i} as well as the liquid–vapor surface tension γ_{s} and the liquid viscosity η. This can be explained by the fact that the strengthen of the liquid properties corresponding to the cohesive and viscous stresses of the binding liquid and the increase in the impact rate leads to the high early-stage forces inside agglomerates [63].

The final-stage deposition behavior of impact agglomerates is also an interesting feature, which we analyze in more detail in order to get a better understanding of the effects of liquid properties and impact velocity on the impact dynamics of spherical agglomerates. We access the final deposition stage of granules by considering its height D_{stop} and the loss

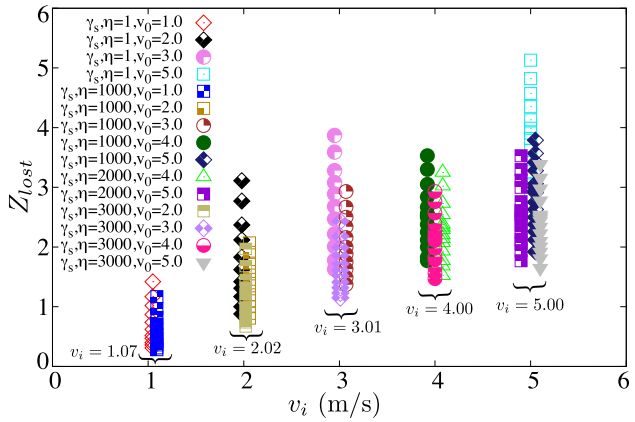

Fig. 10 Average lost coordination number Z_{lost} of wet agglomerates as a function of the impact velocity v_i. The symbols and their colors represent for each value of η and v_i and a broad range of values of the surface tension γ_s of the binding liquid. (Color figure online)

coordination number Z_{lost}. Figure 9 shows the normalized granule height D_{stop}/D_0 at its final deposit step as a function of v_i for different values of γ_s and the liquid viscosity η. This ratio clearly increases proportional to γ_s and η, whereas it declines systematically as a function of the impact velocity v_i.

Figure 10 displays the loss coordination number Z_{lost} at the final deposition stage as a function of the impact velocity v_i for all of our simulations. The increase in the cohesion and the viscosity of the binding liquid leads to reduction in the number of loss capillary bonds, whereas the increase in the impact speed leads to an increase in the average number of loss capillary bridges. We also see that the increase in Z_{lost} is much more significant with v_i than the liquid–vapor surface tension γ_s and the liquid viscosity η. However, there seems to have a unified tendency of the evolution of the plastic strength threshold, the deposition height, and the loss coordination number of wet agglomerates, which could be expected to scale by an appropriate parameter.

4 Power-law scaling behavior

The issue is whether all different data points of the agglomerate strength σ_p/σ_c, the final-stage deposition height D_{stop}/D_0, and loss coordination number Z_{lost} at the final deposition stage of impact agglomerate can be expressed as a collapsed function of a general inertial number that combines the liquid–vapor surface tension γ_s, the liquid viscosity η, and the impact rate $\dot{\gamma} = v_i/D_0$. Before considering this option, we first define two dimensionless numbers in our system: (1) The Capillary number $\text{Ca} = \sigma_v/\sigma_c = \eta\dot{\gamma}\langle d\rangle/\gamma_s$ is a ratio of the viscous stress σ_v and the cohesive stress σ_c and (2) the Stokes number $\text{St} = \sigma_i/\sigma_v = \rho\langle d\rangle^2\dot{\gamma}/\eta$ is a ratio of the inertial stress σ_i to the viscous stress σ_v.

In the steady-state confined shearing flows of unsaturated granular materials, Vo et al. [33] showed that the rheological properties and effective viscosities of such flows can be described as a general inertial number I_m that combines the inertial number I, the cohesion index ξ, and the Stokes number St by considering the additive mechanism of stresses exert on particles. I_m is expressed by the following function:

$$I_m = I\left(\frac{1+\beta/\text{St}}{1+\alpha\xi}\right)^{1/2}, \tag{12}$$

where I denotes the inertial number, defined as a ratio of the relaxation time and the impact time ($I = \dot{\gamma}\langle d\rangle\sqrt{\rho/\sigma_n}$), in which $\dot{\gamma} = v_i/D_0$ is the impact rate of an agglomerate on the flat plane, $\langle d\rangle$ is the mean particle diameter, ρ denotes the particle density, and σ_n is the confining pressure of the confined granular sample, the cohesion index $\xi = \sigma_c/\sigma_n$, defined as a ratio of the cohesion stress σ_c to the confining stress σ_n, and α and β are the pre-factors that depend on material parameters.

However, in our current work, the gravity or the applied confining pressure does not prevail, the cohesive stress largely exceeds the confining stress, and the inertial stress is much more dominant as compared to the viscous stress exerts on particles. Thus, it is advantageous to compare the inertial stress σ_i with the cohesive stress σ_c rather than the confining stress σ_n. This means that the inertial number I in Eq. (12) can be easily replaced by the expression $\sqrt{\text{Ca}\times\text{St}\times\xi}$. Hence, the generalized inertial number is re-expressed as a function of two dimensionless numbers: Ca and St, which we called the Capillary–Stokes inertial number I_{CS} in this impact test:

$$I_{CS} = (\text{Ca}\times\text{St})^{1/2}. \tag{13}$$

Figure 11 shows the normalized strength σ_p/σ_c of wet agglomerates impacting a flat plane as a function of the Capillary–Stokes inertial number I_{CS}, which is independent to the viscosity of the binding liquid, allowing a remarkable collapse of all our simulation data. This observation can be expressed due to the domination of the inertial stress generated from the particle movements in the impact test as compared to the viscous stress of the liquid binding. I_{CS} provides a unified description of the plastic stress threshold by capturing the effects of the particle interactions including cohesive and viscous stresses in addition to the elastic and frictional forces. All the data points are nicely fitted by the following power-law function form:

$$\frac{\sigma_p}{\sigma_c}(I_{CS}) = a_s I_{CS}^2 + b_s I_{CS} + c_s, \tag{14}$$

with $a_s = 95.00$, $b_s = 8.10$, and $c_s = 0.17$. The fitting form reveals the power-law dependence of the mechanical strength

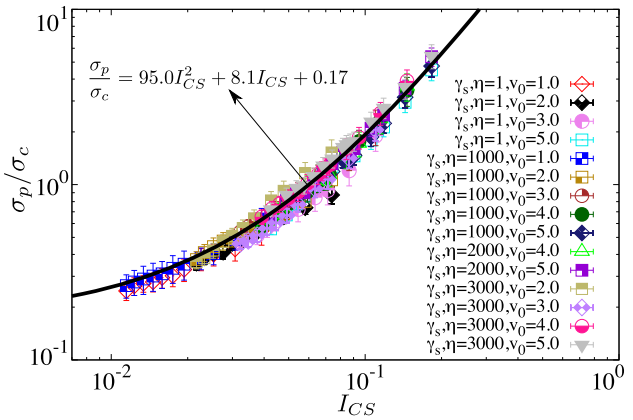

Fig. 11 Normalized strength σ_p/σ_c of wet agglomerates as a function of Capillary–Stokes inertial number I_{CS} defined by Eq. (13), expressed in log–log scale. The error bars represent the standard deviation of the data over the plastic threshold. The symbols and their colors correspond to the parameters that are varied in different ranges. The dark blue line is the functional form of Eq. (14). (Color figure online)

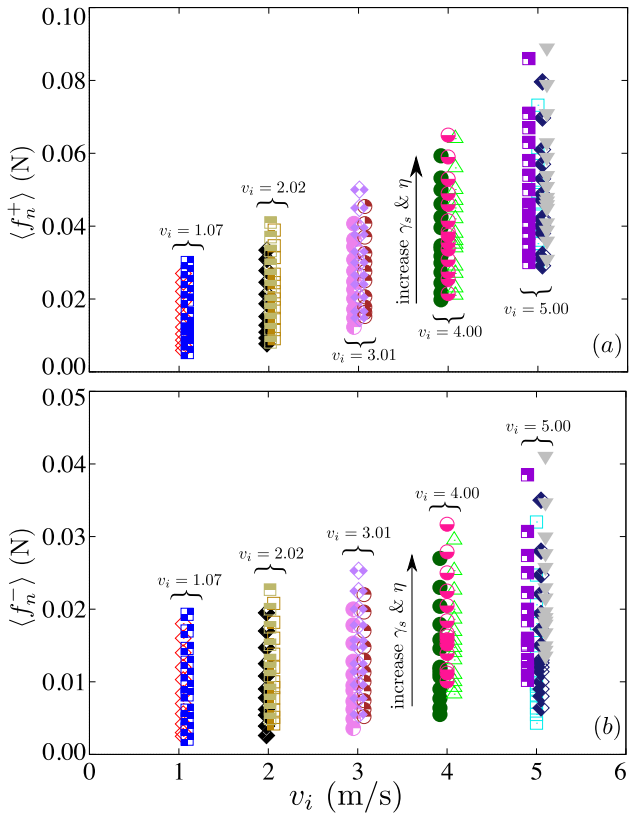

Fig. 12 Mean normal compressive force $\langle f_n^+ \rangle$ (**a**) and mean normal tensile force $\langle f_n^- \rangle$ (**b**) as a function of the impact velocity v_i for all simulations. For each set of simulations, the symbols and their colors (as shown in Fig. 11) correspond to each value of η and v_i and varying γ_s in a broad range of values. (Color figure online)

of wet particle agglomerates on the Capillary–Stokes inertial number.

In order to get a better understanding of the evolution of the normalized peak stress σ_p/σ_c and the scaling behavior of this macroscopic strength of a single wet agglomerate impacting a flat surface, we analyze the micro-mechanical properties of wet granular materials. As previous studies, the macroscopic properties such as the shear strength and packing fraction of granular materials have its microscopic origins [15,38,64–66]. In the current work considering the rapid impact of agglomerates on the rigid plane, the microscopic properties are characterized by the mean normal compressive force $\langle f_n^+ \rangle$ and the mean normal tensile force $\langle f_n^- \rangle$ between primary particles at the peak stage. The compressive forces obtained along the impact direction, whereas the tensile forces have the direction perpendicular to the impact direction, as shown in Fig 3b and c. The normal tensile forces f_n^- shown in this current work are its absolute values. Figure 12a and b displays the evolution of $\langle f_n^+ \rangle$ and $\langle f_n^- \rangle$ as a function of the impact velocity v_i for all our simulations. It is interesting to see that both $\langle f_n^+ \rangle$ and $\langle f_n^- \rangle$ increase with increasing the liquid–vapor surface tension γ_s, the liquid viscosity η, and the impact speed v_i. Remarkably, the mean normal compressive forces $\langle f_n^+ \rangle$ are almost double as compared to the mean normal tensile forces $\langle f_n^- \rangle$, and this means that the macroscopic strength of the agglomerate at its early-stage impact is mainly contributed by the compressive forces between primary particles.

Indeed, Fig. 13a and b shows the normalized mean normal compressive force $\langle f_n^+ \rangle / f_c$ and the normalized mean normal tensile force $\langle f_n^- \rangle / f_c$ between primary particles that increase exponentially as a function of I_{CS}. Meanwhile, $\langle f_n^+ \rangle / f_c$ nicely collapses on a master curve as a function of the Capillary–Stokes inertial number; $\langle f_n^- \rangle / f_c$ does not behave well as a function of the same dimensionless inertial number I_{CS}. In particular, at low values of I_{CS} corresponding to small values of the impact speed and large values of the liquid–vapor surface tension, the normalized mean tensile forces are nearly insensitive. $\langle f_n^- \rangle / f_c$ then separates significantly with large values of I_{CS}. This separation behavior of the mean normal tensile forces may be due to the extension properties of the viscous interactions at high impact rate. Interestingly, the increasing tendencies of $\langle f_n^+ \rangle / f_c$ and $\langle f_n^- \rangle / f_c$ are nearly similar to that of the macroscopic strength of agglomerate at its early-stage impact. Thus, these observations strongly support for the increase and the scaling behavior of the normalized mechanical strength σ_p/σ_c, as presented above.

Although I_{CS} provides a good description of the granule strength and the normal compressive forces at its early-stage impact, it is essential to check its robustness which reflects the final deposition stage of wet agglomerates. As mentioned above, the final deposition stage of agglomerate is characterized by its final-stage deposition height D_{stop} that can be explained by the cumulative loss coordination number Z_{lost}. Figure 14 displays the normalized D_{stop}/D_0 nearly

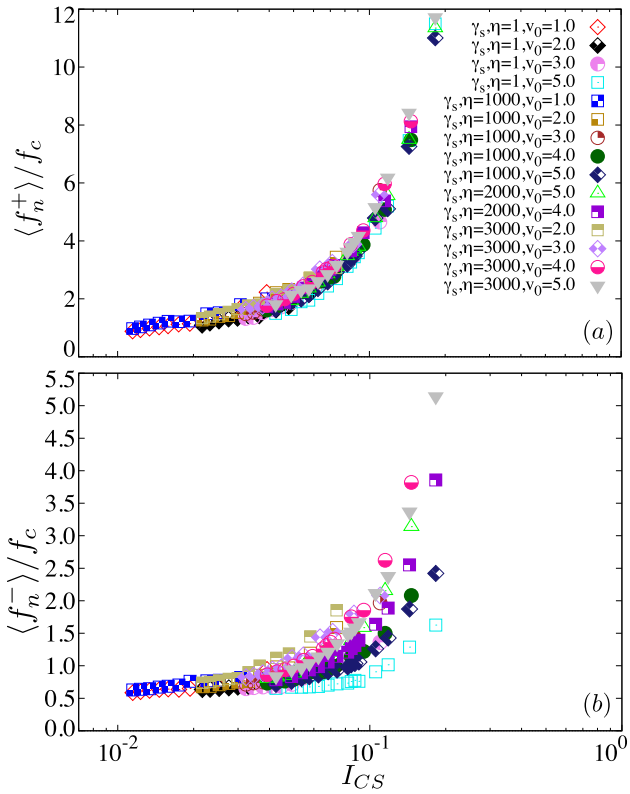

Fig. 13 Normalized mean normal compressive force $\langle f_n^+ \rangle$ (**a**) and normalized mean normal tensile force $\langle f_n^- \rangle$ (**b**) by the cohesion force f_c as a function of I_{CS} for all our simulations

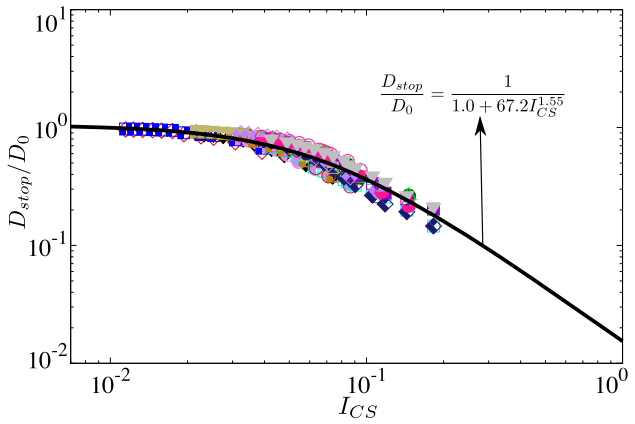

Fig. 14 Normalized vertical diameter at the final deposit stage D_{stop} by initial diameter D_0 of wet agglomerates as a function of Capillary–Stokes inertial number I_{CS} defined by Eq. (13). The symbols and their colors are the same as those in Fig. 11. (Color figure online)

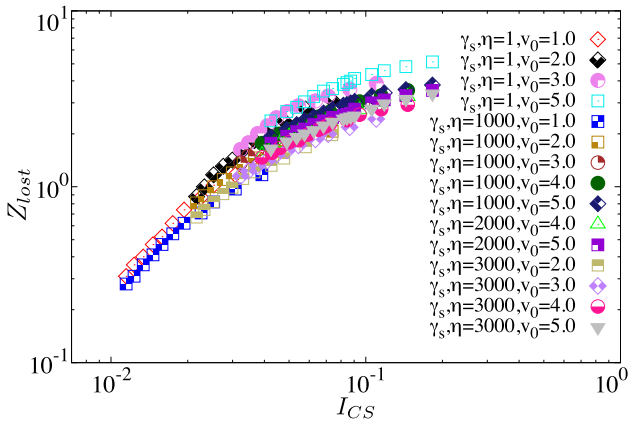

Fig. 15 Cumulative loss coordination number Z_{lost} as a function of Capillary–Stokes inertial number I_{CS}

collapses well on a master curve as a function of the same Capillary–Stokes inertial number I_{CS}. As we can see, the particle agglomerates are nearly insensitive with small values of I_{CS} ($\leq 3 \times 10^{-2}$), and this value can be obtained by choosing appropriate values of the liquid–vapor surface tension and the liquid viscosity as well as controlling an impact velocity that is small enough. The impact agglomerates then rapidly deform as I_{CS} exceeds approximately 3×10^{-2} as a consequence of losing capillary bonds due to the increase in the impact energy. Remarkably, all the data points of D_{stop}/D_0 are nice fitted by the inverse of a power-law function form:

$$\frac{D_{\text{stop}}}{D_0}(I_{\text{CS}}) = \frac{1}{1 + d \times I_{\text{CS}}^{n_{\text{d}}}}, \tag{15}$$

where $d = 67.20$ and $n_{\text{d}} = 1.55$.

Thus, the mechanical strength and the final deposit deformation of agglomerates are nicely scaled as a function of the Capillary–Stokes inertial number. However, the texture variable does not follow this scaling. For example, the cumulative loss coordination number Z_{lost} at the final deposition stage is not scaled by I_{CS} as shown in Fig. 15. This could be explained by the fact that the coordination number or the cumulative loss coordination number affects the granule strength and the final-stage deposition height, but the important parameter is not only the number of contacts or the number of loss capillary contacts but also the orientations and the position of the contacts in the impact test.

5 Conclusions

In this paper, we investigate the dynamic properties and scaling behavior of a single wet particle agglomerate impacting a flat plane by means of 3D discrete element method simulations. The agglomerate is modeled by introducing an approximate analytical expression of the capillary attraction forces and lubrication forces in capillary contacts between particles having the separation distance no exceed the debonding distance in addition to the elastic and frictional forces at their contacts. In this work, we assumed that the liquid is homogeneously distributed in the initial state and irreversibly broken of the capillary bonds during the impact.

In our simulations, we quantified the impact properties of wet agglomerate characterized by the mechanical strength and the microscopic properties at the early-stage impact and the deformation and loss coordination number in the final deposition stage as well as during the impact. We varied systematically broad range of values of three different parameters: (i) the liquid–vapor surface tension γ_s, (ii) the liquid viscosity η, and (iii) the impact velocity v_i by varying the initial velocity v_0.

As expected, the granule represents the ductile behavior and abrupt rupture due to losing capillary contacts and the tensile effects of the capillary bonds. The stress threshold occurs in the early-stage impact, and its values increase proportionally to the liquid–vapor surface tension, the liquid viscosity, and the impact velocity. The increase in the mechanical strength of agglomerates is due to the increase in the normal compressive forces and normal tensile forces between primary particles. The final-stage deposition height and loss coordination number also increase as a function of the impact speed, whereas they decrease proportionally to the cohesion stress and viscous stress of the liquid. Remarkably, by considering the stress additivity in each particle interaction such as cohesive and viscous stresses of the binding liquid in addition to the frictional and elastic forces, the Capillary–Stokes inertial number combining Capillary number and Stokes number nicely scales the granule stress threshold and the final-stage deposition height of agglomerates. By fitting the collapsed data, we determined two power-law function forms. These power-law scalings behaviors are the strong evidence for the role of the liquid properties and the impact speed (or the impact rate) in cohesive granular materials.

To define the scaling parameter (Capillary–Stokes inertial number), we first considered the complex flows of wet granular materials under imposing pressure-controlled condition. In this, the rheology and granular texture of such flows are controlled by the modified inertial number, which combines the inertial number, cohesion index, and the Stokes number by comparing different stresses with the confining stress [33]. However, if the cohesive stress is dominant as compared to the confining stress in our current work, it is essential to check the ratio of the inertial stress and viscous stress to the cohesive stress. As a result, the Capillary–Stokes inertial number was defined by only combining the Capillary number and Stokes number.

Our results presented in this numerical investigation show consistently the ability of our model to handle the dynamic impact of wet particle agglomerates on a flat plane. It can be extended to simulate the diametrical compression test, the impact of agglomerate on the drum walls or the collision between agglomerate and an intruder, in which the behavior of wet agglomerate can provide insight into the evolution of the mechanical strength and the physical properties such as their breakage, deformation, and microstructure. We thus propose these numerical expectations as well as considering the impact experiments to study the mechanical and physical responses of granule.

Acknowledgements This research is funded by Vietnam National Foundation for Science and Technology Development (NAFOSTED) under Grant Number 107.01-2020.24. The authors also gratefully acknowledge Prof. Ha H. Bui for his comprehensive review of this manuscript paper.

Declarations

Conflict of interest The authors declare that there is no conflict of interest.

References

1. Nimmo J (2005) Aggregation|physical aspects. In: Hillel D (ed) Encyclopedia of soils in the environment. Elsevier, Oxford, pp 28–35
2. Sarkar J, Dubey D (2016) Failure regimes of single wet granular aggregate under shear. J Non-Newton Fluid Mech 234:236–248
3. Ennis BJ, Tardos G, Pfeffer R (1991) A microlevel-based characterization of granulation phenomena. Powder Technol 65(1):257–272
4. Rondet E, Delalonde M, Ruiz T, Desfoursb JP (2010) Fractal formation description of agglomeration in low shear mixer. Chem Eng J 164:376–382
5. Barkouti A, Rondet E, Delalonde M, Ruiz T (2012) Influence of physicochemical binder properties on agglomeration of wheat powder in couscous grain. J Food Eng 111:234–240
6. Nosrati A, Addai-Mensah J, Robinson DJ (2012) Drum agglomeration behavior of nickel laterite ore: effect of process variables. Hydrometallurgy 125–126:90–99
7. Chien SH, Carmona G, Prochnow LI, Austin ER (2003) Cadmium availability from granulated and bulk-blended phosphate-potassium fertilizers. J Environ Qual 32(5):1911–1914
8. Suresh P, Sreedhar I, Vaidhiswaran R, Venugopal A (2017) A comprehensive review on process and engineering aspects of pharmaceutical wet granulation. Chem Eng J 328:785–815
9. Lian G, Thornton C, Adams MJ (1998) Discrete particle simulation of agglomerate impact coalescence. Chem Eng Sci 53(19):3381–3391
10. Kafui K, Thornton C (2000) Numerical simulations of impact breakage of a spherical crystalline agglomerate. Powder Technol 109(1):113–132
11. Mishra B, Thornton C (2001) Impact breakage of particle agglomerates. Int J Miner Process 61(4):225–239
12. Thornton C, Ciomocos MT, Adams MJ (2004) Numerical simulations of diametrical compression tests on agglomerates. Powder Technol 140:258–267
13. Liu L, Kafui K, Thornton C (2010) Impact breakage of spherical, cuboidal and cylindrical agglomerates. Powder Technol 199(2):189–196
14. Vo T-T, Mutabaruka P, Nezamabadi S, Delenne J-Y, Izard E, Pellenq R, Radjai F (2018) Mechanical strength of wet particle agglomerates. Mech Res Commun 92:1–7
15. Khalilitehrani M, Olsson J, Rasmuson A, Daryosh F (2018) A regime map for the normal surface impact of wet and dry agglomerates. AIChE J 64(6):1975–1985

16. Vo T-T, Nezamabadi S, Mutabaruka P, Delenne J-Y, Izard E, Pellenq R, Radjai F (2019) Agglomeration of wet particles in dense granular flows. Eur Phys J E 42(9):127
17. Vo T-T, Mutabaruka P, Nezamabadi S, Delenne J-Y, Radjai F (2020) Evolution of wet agglomerates inside inertial shear flow of dry granular materials. Phys Rev E 101:032906
18. Tong Z, Yang R, Yu A, Adi S, Chan H (2009) Numerical modelling of the breakage of loose agglomerates of fine particles. Powder Technol 196(2):213–221
19. Vo TT (2019) Modeling the rheology of wet granular materials. Thesis, Université de Montpellier
20. Talu I, Tardos GI, Khan MI (2000) Computer simulation of wet granulation. Powder Technol 110:59–75
21. Iveson S, Beathe J, Page N (2002) The dynamic strength of partially saturated powder compacts: the effect of liquid properties. Powder Technol 127:149–161
22. Ghadiri M, Salman AD, Hounslow M, Hassanpour A, York DW (2011) Editorial: Special issue—agglomeration. Chem Eng Res Des 89(5):499
23. Nguyen D, Rasmuson A, Thalberg K, Niklasson Björn I (2015) A breakage and adhesion regime map for the normal impact of loose agglomerates with a spherical target. AIChE J 61(12):4059–4068
24. Rahmanian N, Ghadiri M (2013) Strength and structure of granules produced in continuous granulators. Powder Technol 233:227–233
25. Khalifa A, Breuer M (2020) Data-driven model for the breakage of dry monodisperse agglomerates by wall impact applicable for multiphase flow simulations. Powder Technol 376:241–253
26. Ning Z, Boerefijn R, Ghadiri M, Thornton C (1997) Distinct element simulation of impact breakage of lactose agglomerates. Adv Powder Technol 8(1):15–37
27. Thornton C, Ciomocos M, Adams M (1999) Numerical simulations of agglomerate impact breakage. Powder Technol 105(1):74–82
28. Liu L, Thornton C, Shaw SJ, Tadjouddine EM (2016) Discrete element modelling of agglomerate impact using autoadhesive elastic–plastic particles. Powder Technol 297:81–88
29. Deng X, Davé RN (2017) Breakage of fractal agglomerates. Chem Eng Sci 161:117–126
30. Vo T-T (2021) Scaling behavior of the tensile strength of viscocohesive granular aggregates. Phys Rev E 103:042902
31. Zhang L, Wu C-Y (2020) Discrete element analysis of normal elastic impact of wet particles. Powder Technol 362:628–634
32. Chen H, Liu W, Zheng Z, Li S (2021) Impact dynamics of wet agglomerates onto rigid surfaces. Powder Technol 379:296–306
33. Vo T-T, Nezamabadi S, Mutabaruka P, Delenne J-Y, Radjai F (2020) Additive rheology of complex granular flows. Nat Commun 11:1476
34. Radjai F, Topin V, Richefeu V, Voivret C, Delenne J-Y, Azéma E, El Youssoufi MS (2010) Force transmission in cohesive granular media. In: Goddard JD, Jenkins JT, Giovine P (eds) Mathematical modeling and physical instances of granular flows. AIP, Dabaka, pp 240–260
35. Bagnold RA (1954) Experiments on a gravity-free dispersion of large solid spheres in a Newtonian fluid under shear. Proc R Soc Lond 225:49–63
36. da Cruz F, Emam S, Prochnow M, Roux J-N, Chevoir F (2005) Rheophysics of dense granular materials: discrete simulation of plane shear flows. Phys Rev E 72:021309
37. Khalilitehrani M, Olsson J, Daryosh F, Rasmuson A (2019) The morphology of the deposited particles after a wet agglomerate normal surface impact. Powder Technol 345:796–803
38. Azéma E, Sánchez P, Scheeres DJ (2018) Scaling behavior of cohesive self-gravitating aggregates. Phys Rev E 98:030901
39. Vo T-T (2020) Erosion dynamics of wet particle agglomerates. Comput Part Mech 8:601–612
40. Trulsson M, Andreotti B, Claudin P (2012) Transition from the viscous to inertial regime in dense suspensions. Phys Rev Lett 109:118305
41. Amarsid L, Delenne J-Y, Mutabaruka P, Monerie Y, Perales F, Radjai F (2017) Viscoinertial regime of immersed granular flows. Phys Rev E 96:012901
42. Vo T-T (2020) Rheology and granular texture of viscoinertial simple shear flows. J Rheol 64(5):1133–1145
43. Radjai F, Dubois F (2011) Discrete-element modeling of granular materials. Wiley, New York
44. Richefeu V, ElYoussoufi S, Azéma E, Radjai F (2009) Force distribution in cohesive and non cohesive granular media. Powder Technol 190:258263
45. Matuttis H, Luding S, Herrmann H (2000) Discrete element simulations of dense packings and heaps made of spherical and non-spherical particles. Powder Technol 109(1):278–292
46. Lian G, Thornton C, Adams M (1993) A theoretical study of the liquid bridge forces between two rigid spherical bodies. J Colloid Interface Sci 161:138–147
47. Scheel M, Seemann R, Brinkmann M, Michiel MD, Sheppard A, Herminghaus S (2008) Liquid distribution and cohesion in wet granular assemblies beyond the capillary bridge regime. J Phys Condens Matter 20(49):494236
48. Delenne J-Y, Richefeu V, Radjai F. (2015) Liquid clustering and capillary pressure in granular media. J Fluid Mech 762:R5
49. Richefeu V, El Youssoufi MS, Radjaï F (2007) Shear strength of unsaturated soils: experiments, dem simulations, and micromechanical analysis. In: Theoretical and numerical unsaturated soil mechanics. Springer, Berlin Heidelberg, pp 83–91
50. Willett C, Adans M, Johnson S, Seville J (2000) Capillary bridges between two spherical bodies. Langmuir 16:9396–9405
51. Moreno-Atanasio R (2012) Energy dissipation in agglomerates during normal impact. Powder Technol 223:12–18 **(Invited papers from delegates of Chemeca 2010: The 40th Annual Australasian Chemical Engineering Conference)**
52. Cundall PA, Strack ODL (1979) A discrete numerical model for granular assemblies. Géotechnique 29(1):47–65
53. Allen MP, Tildesley DJ (1987) Computer simulation of liquids. Oxford University Press, Oxford
54. Luding S (1998) Collisions and contacts between two particles. In: Herrmann HJ, Hovi J-P, Luding S (eds) Physics of dry granular media—NATO ASI series E350. Kluwer Academic Publishers, Dordrecht, p 285
55. Thornton C (1999) Quasi-static shear deformation of a soft particle system. Powder Technol 109:179–191
56. Duran J, Reisinger A, de Gennes P (1999) Sands, powders, and grains: an introduction to the physics of granular materials, partially ordered systems. Springer, New York
57. Richefeu V, El Youssoufi M, Radjai F (2006) Shear strength properties of wet granular materials. Phys Rev E 73:051304
58. Pitois O, Moucheront P, Chateau X (2000) Liquid bridge between two moving spheres: an experimental study of viscosity effects. J Colloid Interface Sci 231(1):26–31
59. Badetti M, Fall A, Hautemayou D, Chevoir F, Aimedieu P, Rodts S, Roux J-N (2018) Rheology and microstructure of unsaturated wet granular materials: experiments and simulations. J Rheol 62(5):1175–1186
60. Mikami T, Kamiya H, Horio M (1998) Numerical simulation of cohesive powder behavior in a fluidized bed. Chem Eng Sci 53(10):1927–1940
61. Rabinovich YI, Esayanur MS, Moudgil BM (2005) Capillary forces between two spheres with a fixed volume liquid bridge: theory and experiment. Langmuir 21:10992–10997

62. Richefeu V, Radjai F, Youssoufi MSE (2007) Stress transmission in wet granular materials. Eur Phys J E 21:359–369
63. Krizou N, Clark AH (2020) Power-law scaling of early-stage forces during granular impact. Phys Rev Lett 124:178002
64. Azéma E, Radjaï F (2014) Internal structure of inertial granular flows. Phys Rev Lett 112:078001
65. Azéma E, Linero S, Estrada N, Lizcano A (2017) Shear strength and microstructure of polydisperse packings: the effect of size span and shape of particle size distribution. Phys Rev E 96:022902
66. Cantor D, Azéma E, Sornay P, Radjai F (2018) Rheology and structure of polydisperse three-dimensional packings of spheres. Phys Rev E 98:052910